



Unione Europea
Fondo Europeo di Sviluppo Regionale



ClimOpt

Ottimizzazione della gestione dei rischi climatici

Programma: Interreg IV A Italia-Svizzera

- **Extension of Adige River Flood Forecasting System for debris flow forecasting, simulation of glacial hydrology and artificial reservoir storage accounting**

AUTONOME
PROVINZ
BOZEN
SÜDTIROL



PROVINCIA
AUTONOMA
DI BOLZANO
ALTO ADIGE



KANTON
GRAUBÜNDEN
AMT FÜR WALD
UND NATURGEFAHREN



Editore: Provincia autonoma di Bolzano – Alto Adige e Cantone dei Grigioni

Provincia autonoma di Bolzano – Alto Adige

Ripartizione Protezione antincendi e civile, viale Druso 116, 39100 Bolzano
protezione.antincendiecivile@provincia.bz.it, www.provincia.bz.it/protezione-civile
Direttore di ripartizione Hanspeter Staffler

Cantone dei Grigioni

Ufficio foreste e pericoli naturali, via Loë 14, CH-7000 Coira
info@awn.gr.ch, www.awn.gr.ch
Capo settore Christian Wilhelm

© 2014

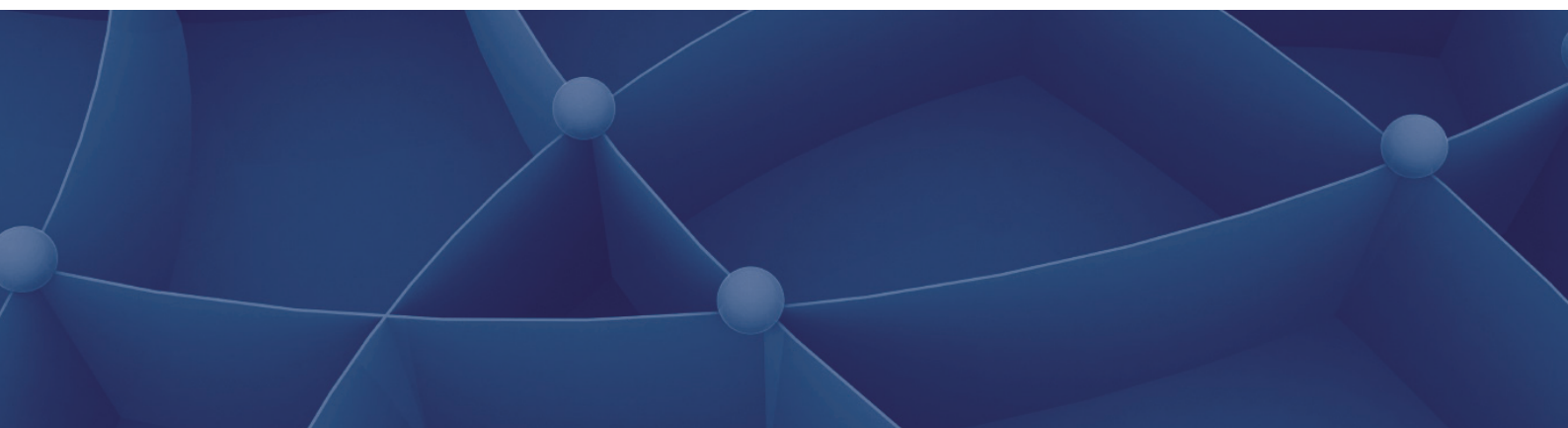
Coordinamento progetto

Andreas Zischg (abenis alpinexpert srl/abenis AG)
a.zischg@abenis.it, www.abenis.it, www.abenis.ch
Roberto Dinale (Ufficio idrografico della Provincia autonoma di Bolzano)
roberto.dinale@provincia.bz.it, www.provincia.bz.it/hydro

Grafica

sonya-tschager.com

Ristampa permessa soltanto con autorizzazione dell'editore



ClimOpt – Ottimizzazione della gestione dei rischi climatici
Interreg Italia-Svizzera 2007-2013

Autore:

Marco Borga

Co-autori:

E. Nikolopoulos, D. Zoccatelli, F. Marra

31 agosto 2014



Unione Europea
Fondo Europeo di Sviluppo Regionale



Le opportunità non hanno confini.



Summary

This report provides a summary of the work carried out by UNIPD and ATSOFT aimed at the updating of several hydrological procedures in the Adige River Flood Forecasting System (ARFFS). The work is splitted into the three following sections:

- Definition of precipitation thresholds and of model-based soil moisture simulation tools for debris flow forecasting;
- Extension of ARFFS to the simulation of hydrological processes in glacier mountain basins;
- Extension of ARFFS to the simulation of flood simulation in artificial reservoir systems.

Index

1.	Introduction	6
2.	Definition of precipitation thresholds and soil moisture simulation tools for debris flow forecasting	7
2.1	Introduction	7
2.2	Study area, data and raingauge-based ID thresholds	7
2.3	Radar-based ID thresholds	11
2.4	Soil moisture and debris flow triggering – deriving soil moisture information by means of ICHIMOD	18
3.	Extension of ICHYMOD to the simulation of glaciated catchmenst	24
3.1	Snow / Glacier routine for ICHYMOD	24
3.2	Model implementation	27
4.	Extension of ICHYMOD to the simulation of artificial reservoir systems.....	30
	References	31



1. Introduction

This report provides a summary of the work aimed at the updating of several hydrological procedures in the Adige River Flood Forecasting System (ARFFS). The work is splitted into the following sections:

- Definition of precipitation thresholds and of model-based soil moisture simulation tools for debris flow forecasting;
- Extension of ARFFS to the simulation of hydrological processes in glacier mountain basins;
- Extension of ARFFS to the simulation of flood simulation in artificial reservoir systems.



2. Definition of precipitation thresholds and soil moisture simulation tools for debris flow forecasting

2.1 Introduction

Debris flows are rapidly flowing, gravity-driven mixtures of roughly equal parts of sediment and water in which a broad distribution of grain size, commonly including gravel and boulders, is mixed vertically (Iverson, 2005).

Considerable research efforts have been made so far to determine the rainfall amount required for rainfall-induced landslides or debris flows (Salvati et al., 2010). Rainfall thresholds are often used to identify the local or regional rainfall conditions that, when reached or exceeded, are likely to result in landslides or debris flows (e.g., Caine, 1980; Wieczorek, 1996; Jakob et al., 2012). Following the pioneering works of Caine (1980), rainfall thresholds for shallow landslides and debris flows (collectively termed ‘debris flows’ hereinafter) were determined at the local, regional, and global scales. Guzzetti et al. (2008) proposed a review of the literature on rainfall thresholds for the possible initiation of debris flows.

This report provides a summary of three specific research efforts aimed at: i) define the precipitation thresholds based on the ED30 debris flow archive 1999-2012; ii) define the precipitation thresholds for a selected number of debris-flow triggering storm, for which radar data are available; iii) analysis of soil moisture space-time variability simulated by ARFFS and comparison with satellite-based soil moisture estimates.

2.2 Study area, data and raingauge-based ID thresholds

The data used for this study were obtained in the Upper Adige River basin, a mountainous region covering approximately 7,400 km² in Northern Italy (**Fig. 1**). This region has been selected based on three motivations. First, Salvati et al. (2010) have recognized that this area was characterized by a significant societal landslide risk in the period 1950–2008. Second, a database listing more than 400 debris flows in the period 2000–2010 is available for the area. Third, the area is equipped with a dense network of raingauges, which is a necessary condition for the examination of the rainfall sampling problem.

Elevation in the area ranges between 200 and 3,900 m a.s.l, with mean elevation around 1,800 m a.s.l. The precipitation regime is influenced by western Atlantic airflows and southern circulation patterns (Norbiato et al., 2009a). The dominant climate pattern in the region is continental, with the distribution of the monthly precipitation showing two maxima, in August and October. Cold months (from October to April) are dominated by snow, and widespread precipitation. Between May and September, the precipitation is brought by mesoscale convective systems and localized thunderstorms (Norbiato et al., 2009a; Mei et al., 2014). Part of



the western portion of the study area belongs to the dry internal alpine region, with a mean annual precipitation (MAP) ranging between 400 mm and 700 mm, the result of sheltering of the mountain range to southerly and northerly winds. The MAP increases to 1,300 mm in the Northern portion of the region, where the rainfall regime is conditioned by the “*stau*” effect i.e., the intensification of rainfall when warm and moist air from the Mediterranean Sea is lifted over the Alps, leading to the foehn effect on the leeward side. The dry-to-moderate rainfall regime is reflected also in the climatology of the rainfall extremes. Rainfall quantiles corresponding to a 100-year return period rarely exceed 50 mm at 1-hour duration, and 150 mm at 24-hour duration (Norbiato *et al.*, 2009b).

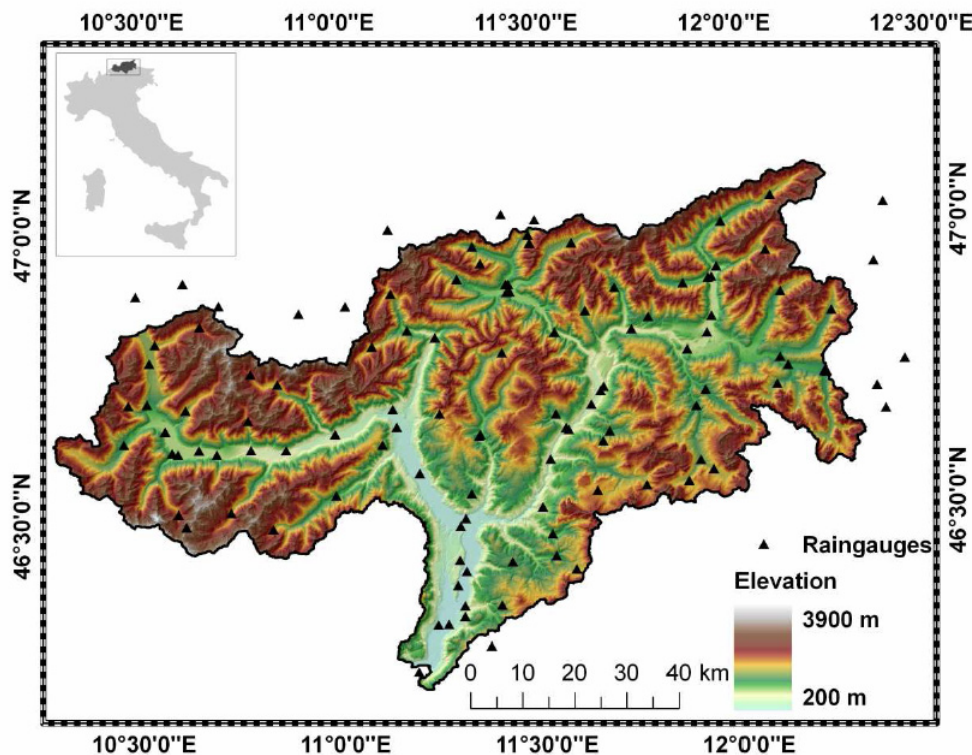


Fig.1: Study area and raingauges used in the analysis

In 1998, the local Government (Alto Adige-Southern Tyrol Province) began a systematic collection of information on the occurrence of debris flows in the Upper Adige River basin. This long-term effort has resulted in the compilation of the ‘Event Documentation 30’ (ED30) database listing information on the location of 442 debris flows in the period 2000–2010. In the database, the initiation point of the individual debris flows is geo-referenced with accuracy up to 50 m. The database is considered complete, except for a systematic censoring of very small (< 700 m³) failures that remained hidden under the forest canopy, or stopped upstream from the debris flow fans (Brardinoni *et al.*, 2012). This is an unprecedented detail for catalogues of historical landslide events (Pavlova *et al.*, 2011). Examination of the seasonal distribution of



the debris flows listed in the database revealed that 90% of the events occurred between June and September, a seasonal period when precipitation is dominated by rainfall, and snowfall is rare. Based on this evidence, we excluded from the analysis all the events in the catalogue that have occurred between October and May. The reduced dataset lists 405 debris flows, whose geographical location is shown in **Fig. 2**.

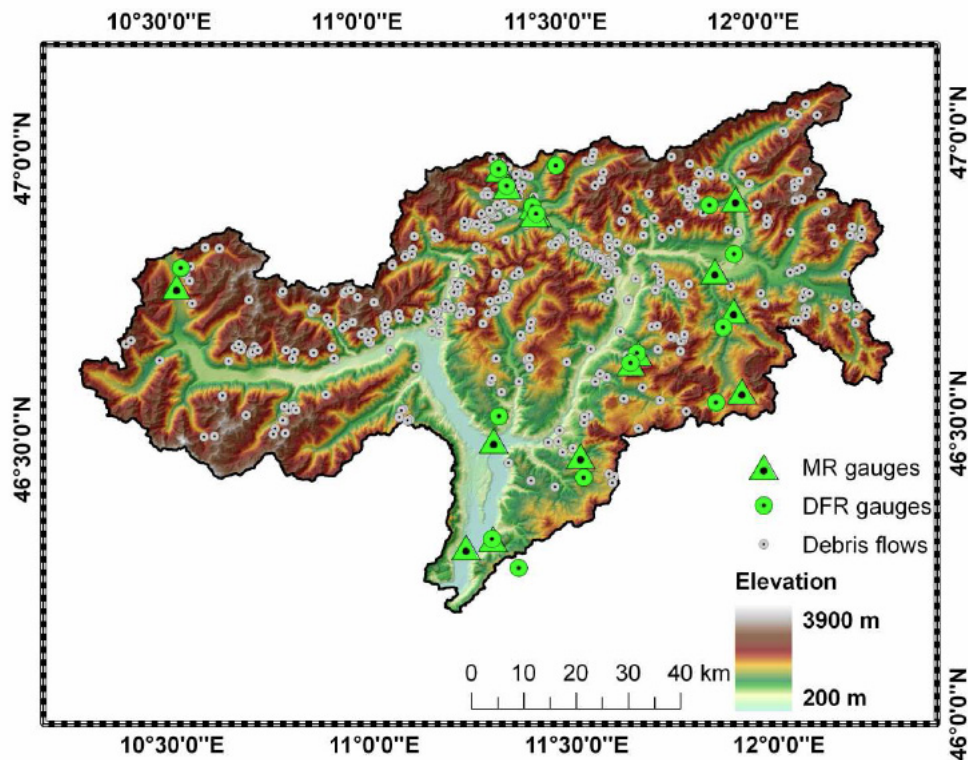


Fig.2: Study area and raingauges with location of the DF.

A dense network of raingauges measures the precipitation in the study area (**Fig. 2**), including 100 raingauges located inside the basin area (60 raingauges with data available for at least 90% of the time over the study period 2000-2010). This corresponds to a density of about one raingauge every $\sim 74 \text{ km}^2$. The horizontal distance between two neighbouring raingauges ranges from 0.44 km to 15.3 km, with an average of 5.8 km. The altitude of the raingauges ranges from 200 m a.s.l. to 2800 m a.s.l., with an average of 1200 m a.s.l. The temporal resolution of the original data is ten minutes; the data have been aggregated at the hourly resolution for the analyses described below.

To estimate the regional rainfall intensity-duration threshold we adopted the *frequentist* method proposed by Brunetti et al., (2010). The method allows one to define *ID* rainfall thresholds characterized by different levels of exceedance probabilities (e.g. 1% and 5% are commonly used exceedance levels, see for example Brunetti et al. (2010), Peruccacci et al. (2012)). In this work, we used the 1% exceedance probability level to estimate the rainfall threshold, which



means that the probability of a debris flow triggering rainfall event (I, D pair) to be under the estimated ID threshold is less than 1%. For each recorded debris flow date and location, the corresponding rainfall event was determined at the closest raingauge, using the available rainfall record, and the values of the rainfall duration and of the mean rainfall intensity was calculated. Calculation of event-based properties required the identification of the individual rainfall events in the rainfall records. Separation of subsequent rainfall events was based on the use of an inter-event period of 24 consecutive hours without rainfall. **Fig. 3** summarizes the I, D pairs for the 405 debris flows analysed in this study, and the corresponding ID threshold, $I = 1.12 D^{-0.49}$, with I in mm h^{-1} and D in hours. The estimated exponent $\beta = 0.49$ is close to the exponents for other ID thresholds proposed in literature for areas in northern Italy (e.g., Guzzetti et al., 2007, and references therein), but the multiplier α is considerably lower suggesting that the rainfall required to trigger debris flows in the Upper Adige River basin is less than in other areas of northern Italy. The difference can be the result of a number of factors, including the variability of the physical factors that control debris flow initiation (e.g., lithology, topography, soil type, vegetation cover) in the different areas and the less intense rainfall regime in the study area. The availability of a very detailed catalogue of debris flows may also lead to differences in the ID estimation.

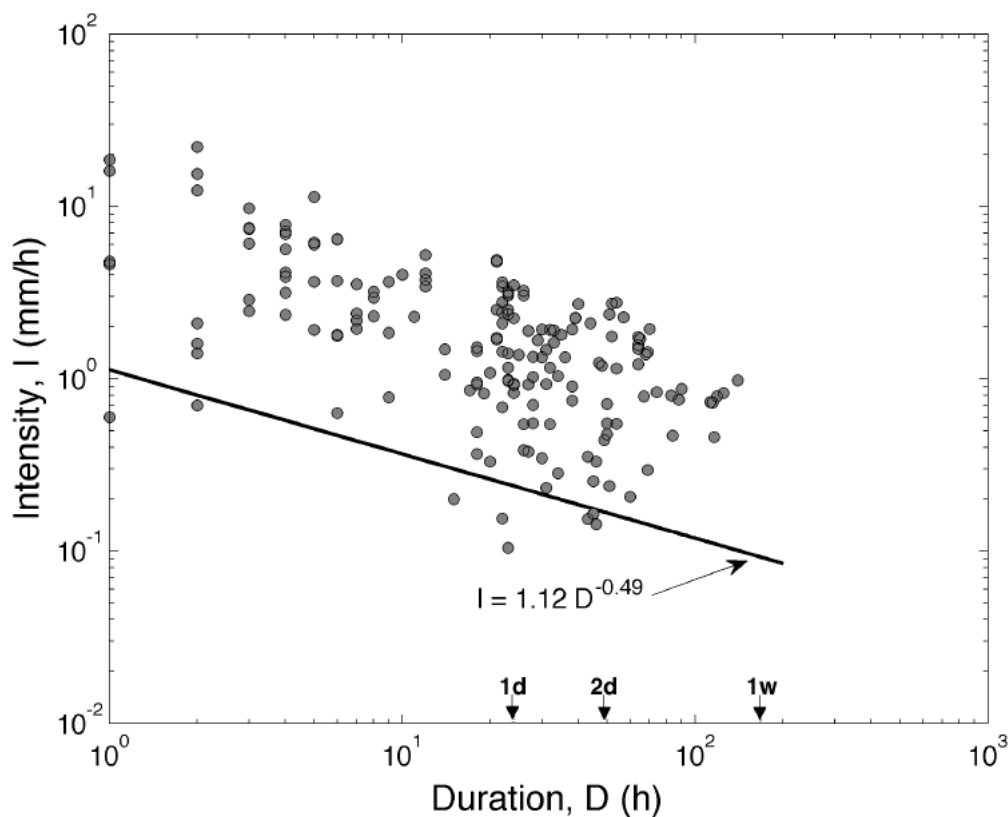


Fig.3: Rainfall duration (D , in hours) and mean rainfall intensity (I , in mm/h) values of recorded debris flow triggering rainfall events, according to closest available gauge observations. Black line is the estimated ID rainfall threshold at 1% exceedance level.



2.3 Radar-based ID thresholds

Rainfall intensities and durations used to identify the *ID* threshold are generally obtained through spatial estimation (see Section 2.2). When rainfall properties are estimated according to the available raingauges, errors are introduced in the assessment of the rainfall intensities and durations over debris flow locations. The sources of uncertainty in spatial estimation of rainfall are related to: (i) density and geometry of the gauge networks (Morrissey et al., 1995), (ii) estimation procedures (Tabios and Salas, 1985), and (iii) spatial variability of rainfall (Marra et al., 2014). For the specific problem of ID threshold identification, errors in rainfall estimates translate in error in the estimated *ID* threshold. **Fig. 4** provides a graphical example of the rainfall error propagation in the estimation of an *ID* threshold, given an ideal condition of clear separation between rainfall that have triggered (black dots) and have not triggered (white dots) debris flows (**Fig. 4a**). This *ID* threshold is termed here ‘true’ threshold. The effect of the rainfall estimation uncertainty of the identification of the *ID* threshold (**Fig. 4a**) is shown in **Fig. 4b**. Essentially, some rainfall intensities will be underestimated and others will be overestimated, resulting in the collapsing of the clear separation (ideal case) and the mixing of debris and no-debris flow events. Given that the ID threshold is estimated as a lower boundary of the estimated debris flow triggering rainfalls, it is expected that the uncertainty in rainfall estimation will lead to a biased identification of the *ID* threshold. Biases due to orographic dependence of the debris-flow triggering rainfall may add to this bias. Therefore the effects listed above will translate to biased estimation of the α and the β parameters in the *ID* threshold eq. (1).

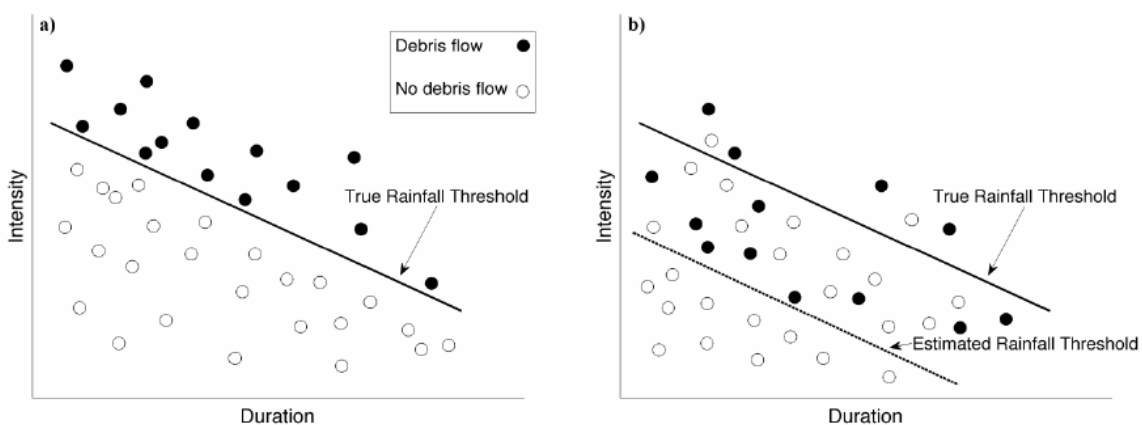


Fig. 4: Conceptual description of the effect of rainfall estimation uncertainty on the *ID* threshold model estimation. (a) Ideal condition in which there is a clear separation between rainfall that triggered (black dots) and did not triggered (white dots) debris flows; (b) representation of ideal conditions in (a) affected by uncertainty in rain estimation.

A potential solution to the observational limitations posed by raingauges, lies on remote-sensing observations, and more specifically on weather radar rainfall estimates. Compared with the sparse distribution of raingauges, the high spatial and temporal resolutions of radar-observed



rainfall fields are highly desirable for debris flows and landslide studies, since they offer the unique advantage of estimating rainfall over the actual debris flow location (David-Novak et al., 2004; Chiang and Chang, 2009). The vast advancements of weather radar technology over the last decades enabled the use of these data sources for debris flow warning procedures. However, several factors, both instrumental and meteorological, affect the accuracy of radar-rainfall estimates in mountainous areas (Germann et al., 2006). A number of correction procedures have been proposed and tested for the main sources of errors, mainly for applications concerning the rainfall estimation for flood and flash flood forecasting (Villarini and Krajewski, 2010; Gourley et al., 2011). Nevertheless, radar-based estimation of debris-flow triggering rainfall may pose different challenges with respect to those characterizing more common hydrological applications. These differences are largely related to the small size of debris flow catchments (sometimes even less than 1 km², D'Agostino and Marchi, 2001) relative to those involved in flood-related phenomena, which are usually larger by at least an order of magnitude. Owing to the small size of the basin area, the random component of the error may have a larger impact on the total radar-rainfall estimation error. Moreover, considering that debris flows scales are comparable to single radar pixel, it is expected that radar beam pointing errors may have an important effect on estimating the actual triggering rainfall properties. This is further reinforced if we take into account that debris flow triggering events are often characterized by high precipitation gradients (i.e. rainfall spatial variability) (Nikolopoulos et al., 2014). The specific objective of this Section is to assess the performance of the radar rainfall estimates, either adjusted and not by using raingauge data, for *ID* threshold identification. Most of the work is taken by Marra et al. (2014).

Seven debris-flow triggering rainfall events that occurred in the study area between 2005 and 2012 are examined. Those events are among the most severe in the region during this period and triggered a total of 117 debris flows that caused significant damage to people and infrastructures. Tab. 1 summarizes the characteristics of the rainfall events.

Tab. 1: Characteristics of the rainfall events examined.

Date	Number of triggered debris flows	Event duration [h]	Number of raingauges	Max. raingauge rainfall accumulation [mm]	Max. raingauge hourly rainfall [mm h ⁻¹]
August 1, 2005	5	2	7	5.6	5.6
June 20-21, 2007	13	20	14	102.1	25.8
July 16-17, 2009	7	27	8	150.1	95.5
July 30, 2009	15	9	14	54.0	53.0
September 4, 2009	6	12	17	122.5	23.8
August 14-15, 2009	7	13	25	160.1	47.4
August 4, 2012	64	8	8	86.0	30.6



The events all occurred during the summer months with three events in August, two in July and one in June and September. As such, these events are deemed to be representative of the summer season debris flows triggering storm systems in the region. For each event, an area ranging in size from 290 to 900 km² was identified, large enough to include the rainfall event, the triggered debris flows and the closest raingauge to each debris flow initiation point. The raingauge data were carefully examined, rejecting from the analysis the raingauges that reported suspicious data. The duration of the storms varies from 2 h (August 1, 2005) to 27 h (July 16-17, 2009) with maximum event cumulated raingauge-rainfall ranging between 5.6 mm and 160.1 mm and maximum hourly raingauge-rainfall ranging between 5.6 mm h⁻¹ and 95.5 mm h⁻¹. The distance from the radar site to the study areas is less than 60 km for six events over seven. For one case (August 1, 2005) the range distance is between 75 and 80 km. In all cases, range distance and radar beam shielding errors associated to the two lowest radar beam elevations are such to permit a reasonably successful correction of radar errors.

Radar rainfall estimation methodology

Quantitative rainfall estimation at the ground based on reflectivity observations taken from the Mt. Macaion weather radar presents the usual challenges, which characterize radar rainfall estimation in a mountainous context (German et al., 2006). Significant problems arise from strong echoes where the main lobe or side lobes of the radar beam hit the ground (ground clutter), and from shielding of the radar beam by the horizon. Other error sources affect radar rainfall estimation, including vertical profile of reflectivity, signal attenuation in heavy rain, signal attenuation by water on the radome, variations in rain-drop size distributions.

Radar data are corrected considering the effects of four sources of error: i) signal attenuation in heavy rain, ii) wet radome attenuation, iii) beam shielding, and iv) vertical profile of reflectivity. Moreover, the antenna pointing accuracy is verified by cross-correlating in polar coordinates the observed and simulated ground clutter reflectivity fields. This adds to the conventional sun-tracking method to adjust the pointing accuracy of the radar antenna. The reflectivity-to-rain rate ($Z-R$) relationship used in this work ($Z=308 \cdot R^{1.5}$) has been verified for other isolated convective events observed by the Mt Macaion weather radar. Finally, the corrected radar-rainfall fields are adjusted according to the mean field bias derived on an event-basis, using all the available raingauge rainfall measurements, including those not available in real time conditions.

Overall, it is worth to note that the chain of correction algorithms aims to provide accurate re-analysis data, capitalizing on the additional raingauge data that may not be available in real time and on the retrospective nature of the analysis. This allows for identification, correction, and quantification of the errors, which are generally unfeasible under real time conditions due to insufficient time, data and computational power.

The algorithms used for the correction of the radar-rainfall estimation errors are described below. **Signal attenuation in heavy rain.** Signal attenuation in heavy rain is corrected using the Mountain Reference Technique, based on the procedure reported in Bouilloud et al. (2009). The technique exploits variations in ground clutter return to estimate the total attenuation along



the path (Path Integrated Attenuation), assuming the reflectivity-attenuation relationship to be known. The main advantage of this procedure is that it avoids the numerical instabilities that affect the classical correction techniques. The maximum atmospheric attenuation was observed in presence of the highest rain rates with Path Integrated Attenuation reaching up to 12 dB for the July 16-17, 2009 event.

Wet radome attenuation. Some of the studied events were characterized by heavy rain over the radar antenna, so it is important to check and correct for wet radome attenuation, which may be an important source of error at C-band. To account for this, the same technique used for the signal attenuation is adapted to correct for wet radome attenuation, following the procedure reported in Marra (2013). The method is based on comparing reflectivity of dry ground echoes in presence and absence of rainfall over the radome and exploits the rain data available for the antenna site. A number of ground clutters are identified over the study area for the purpose of this correction. During the September 4, 2009 event a period of severe radome attenuation was clearly identified, with a two-way radome attenuation of 2.7 dBZ.

Beam shielding. Beam shielding occurs when the radar beam hits an obstacle (mountain, antenna towers, etc), and its propagation is partially or totally shielded. For partial beam shielding, it is possible to correct the radar estimates once the fraction of the pulse volume that is visible from the radar antenna is computed. Numerical simulations of radar beam propagation over a digital terrain model of the radar domain (Pellarin et al., 2002) are used to compute the fraction of the pulse volume that is visible. These factors are then used to correct for the shielding error, by limiting the correction to a shield percentage below 70%. This limit is substantially larger than others proposed in the literature (Krajewski et al., 2006); however, the experience gathered with this correction procedure in the study area (Marra, 2013) has shown that potential errors are less important than those due to the use of higher, less shielded pulse volumes, affected by vertical variation of reflectivity.

Vertical Profile of Reflectivity (VPR). Because of beam shielding, earth curvature, and finite beam width, the radar cannot observe precipitation immediately above ground. At 2° beam elevation, which is free from shielding for a large percentage of the radar domain, 40% of the radar measurements are at more than 1.5 km above the terrain. When extrapolating these radar measurements from aloft down to the ground to estimate surface rainfall rates, we need to account for the vertical variation of reflectivity (the Vertical Profile of Radar Reflectivity). This variation is related to processes like growth of precipitation and phase change. For the contrasted rainy system considered here, characterized by convective and stratiform regions, the combination of the vertical (VPR) and radial (attenuation, screening) sources of heterogeneity yields a very challenging problem. To correct for VPR, we used the inverse procedure developed by Andrieu and Creutin (1995). Due to the limited spatial and temporal extension of the studied events, the procedure has been applied to retrieve a representative vertical profile at the event scale accumulation.

Mean field bias adjustment. To correct for remaining biases related to radar electronic calibration and errors in the Z-R relationship, a mean field bias (Berne and Krajewski, 2013) is



computed on an event-accumulation. The radar estimates are adjusted by multiplication by the inverse of the Bias factor.

Radar rainfall estimation scenarios

In the study, four radar rainfall estimation scenarios of incremental complexity are evaluated by using the rain gauge observations as a benchmark for the seven debris-flows triggering storms. In order to permit evaluation of situations where raingauge data may be unavailable for radar processing, which is not uncommon given the limited spatial extension of such rainfall events, two scenarios are obtained without using raingauges for radar adjustment. Rainfall estimates from all radar-rainfall scenarios and available raingauges are used to identify *ID* thresholds for the occurrence of debris flows by using the method proposed by Brunetti et al. (2010), and expanded by Peruccacci et al. (2012). The four scenarios are described below. A description on how each radar rainfall scenario is obtained is provided below.

Scenario I - Raw radar rainfall. This scenario involves the simplest procedure to produce radar rainfall estimates; reflectivity is directly converted into rain rate using the *Z-R* relationship mentioned above. Rainfall estimates are obtained from the lowest least shielded elevation scan available, which means that for each polar element the lowest radar beam elevation is selected which is characterized by a maximum shielding effect. The threshold on the shielding effect was chosen at 30%. This choice permits the use of the first two lowest elevations for the seven events analyzed here. This scenario may be easily implemented in real time; however, the resulting rainfall estimates may be significantly affected by errors not taken into account in the scenario.

Scenario II - Raw radar rainfall adjusted for mean field bias. This scenario involves the mean field bias adjustment of radar rainfall fields of scenario I. As for scenario I, computational requirements are minimal; moreover, the obtained rainfall accumulations are unbiased with respect to raingauge measurements. However, this procedure is conditional to the availability of raingauges and the quality of the rainfall spatial patterns remains the same as with scenario I.

Scenario III - Corrected radar rainfall. Radar observations selected from the two lowest radar beam elevations are corrected using the complete chain of algorithms described above, with the exclusion of mean field bias adjustment. The major advantage of this method is that it can be applied unconditionally to raingauge availability. However, the complexity of the computational sequence prevents its use in real time; moreover, a bias on average rainfall amount may still arise.

Scenario IV - Corrected radar rainfall adjusted for mean field bias. This scenario offers the advantages of scenarios II and III combined: accuracy in the identification of rainfall spatial patterns and unbiased rainfall accumulations. The disadvantages are that a complex elaboration procedure is required and the raingauge data are needed.

Comparison with raingauge rainfall data shows that Scenario IV is characterized by the higher accuracy. This scenario is therefore used to derive a reference rainfall *ID* (Intensity-Duration) relationship (Fig. 5). The reference *ID* is $I=8.57 D^{-0.48}$ (Fig. 9) and is identified by using the *frequency* method at 5% exceedance level (Brunetti et al., 2010).

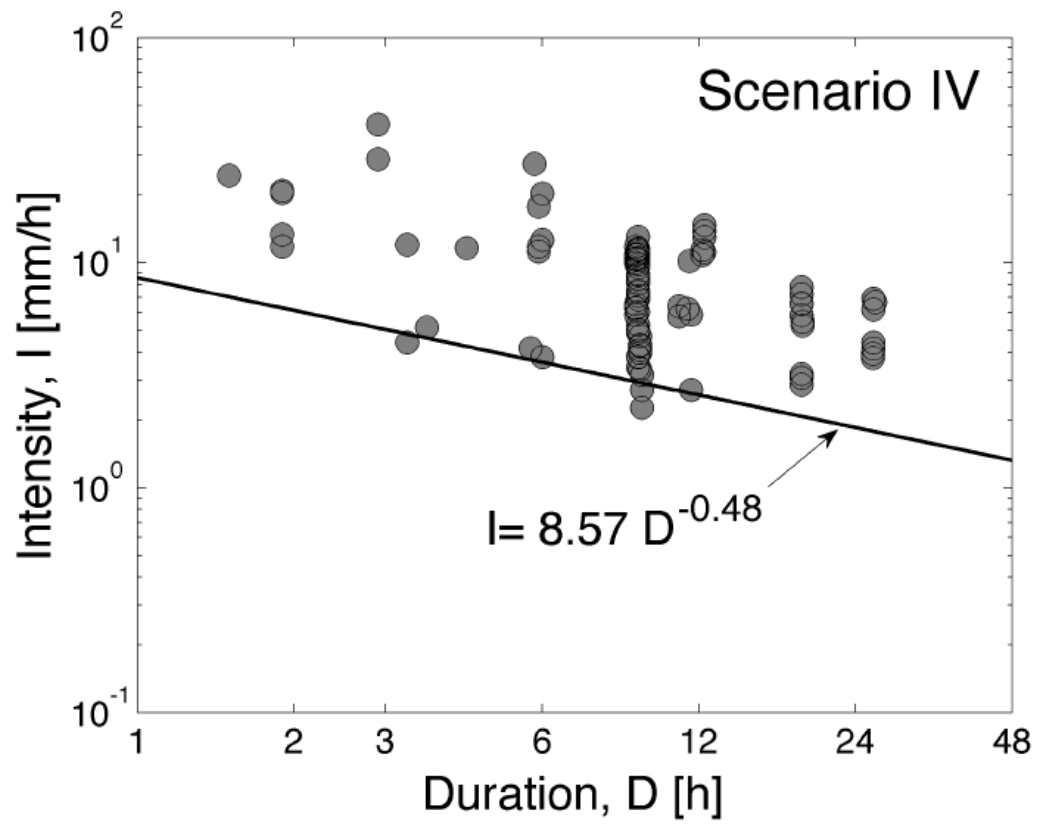


Fig. 5: Intensity-Duration threshold derived from scenario IV.

The identified *ID* thresholds for the three radar rainfall scenarios I to III and raingauges are shown in Fig. 6. In all cases the reference *ID* (scenario IV) is superimposed for comparison.

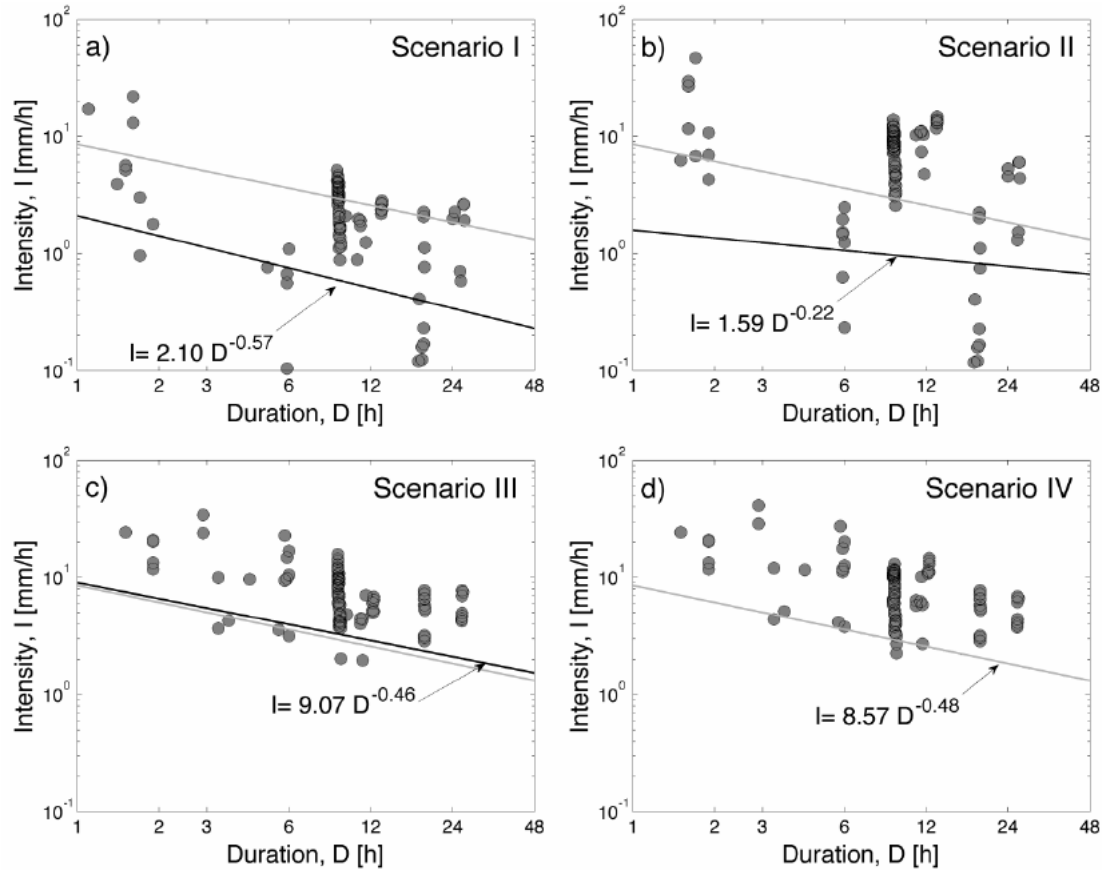


Fig. 6: Intensity-Duration thresholds derived from radar rainfall scenario I to IV (a-d), from the radar pixel located at debris flows locations. The grey line represents the reference threshold (scenario IV).

Results reported in Fig. 6 show that raw radar rainfall estimates identify a threshold which is significantly lower than the one identified from the reference scenario, but characterized by a similar slope ($I = 2.10 \cdot D^{-0.57}$). The implementation of the correction procedures leads to an ID threshold almost undistinguishable from the reference scenario, despite the residual underestimation: $I = 9.07 \cdot D^{-0.46}$. This suggests that carefully corrected radar estimates may be used without application of raingauge-based adjustment for the purpose of ID identification. The comparison of the reference ID with the corresponding one obtained based on raingauge data and on co-located radar observations shows that the main source of difference is related to the rainfall spatial variability and the sampling effect. Raingauge based rainfall measurements identify a threshold curve which is characterized by severe underestimation of both parameters: $I = 2.84 \cdot D^{-0.26}$. This is consistent with findings reported by Nikolopoulos et al. (2014).



2.4 Soil moisture and debris flow triggering – deriving soil moisture information by means of ICHIMOD

It is hypothesized that critical rainfall characteristics (intensity and duration) that trigger shallow landslide/debris flow events, depend also on the spatiotemporal dynamics of soil moisture. The objective in this Section is to investigate this hypothesis and establish under which condition soil moisture play an important role. To investigate this we will analyse here the soil moisture information simulated from the ICHIMOD hydrologic model, the continuous hydrological model used in the frame of ARFFS.

ICHIMOD is the name of the the continuous hydrological model used in ARFFS. This is a conceptual, semi-distributed rainfall-runoff model (Borga, 2002; Borga et al., 2006; Norbiato et al., 2007, 2008, 2009). The model runs on a hourly time step and consists of a snow routine, a soil moisture routine and a flow routing routine. The snow routine represents snow accumulation and melt by using a distribution function approach based on a combined radiation index degree-day concept. Catch deficit of the precipitation gauges during snowfall is corrected by a snowfall correction factor (SCF). A threshold temperature interval is used to distinguish between rainfall, snowfall and a mix of rain and snow. Potential evapotranspiration is estimated by using the Hargreaves method.

The soil moisture routine uses a probability distribution to describe the spatial variation of water storage capacity across a basin. Saturation excess runoff generated at any point in the basin is integrated over the basin to give the total direct runoff entering the fast response pathways to the basin outlet. Drainage from the soil enters slow response pathways. Storage representations of the fast and slow response pathways yield a fast and slow response at the basin outlet which, when summed, gives the total basin flow. The Probability Distributed Moisture (PDM) model configuration used here employs a Pareto distribution of storage capacity, c (Moore, 1985). This has the distribution function

$$F(c) = 1 - \left[1 - (c/c_{max}) \right]^b \quad (1)$$

where c_{max} is the maximum storage capacity in the basin and the parameter b controls the degree of spatial variability of storage capacity over the basin. The instantaneous rate of fast runoff generation from the basin is obtained by multiplying the rainfall rate by the proportion of the basin which is saturated. Saturation excess runoff generated at any point in the basin is integrated over the basin to give the total direct runoff entering the fast response pathways to the basin outlet. Drainage from the soil enters slow response pathways. Storage representations of the fast and slow response pathways yield a fast and slow response at the basin outlet which, when summed, gives the total basin flow.

Losses due to evapotranspiration are calculated as a function of potential evapotranspiration and the status of the soil moisture store. Drainage to the slow flow path is represented by a



function of basin moisture storage and the slow or base flow component of the total runoff is assumed to be routed through an exponential store. Direct runoff from the proportion of the basin where storage capacity has been exceeded is routed by means of a geomorphology-based distributed unit hydrograph (Da Ros and Borga, 1997). For model application, the topography is represented by using Digital Elevation Model (DEM) data.

The Shuffled Complex Evolution optimisation method was used in combination with manual calibration to estimate the hydrological model parameters over the 38 catchments where simulated discharge data can be compared with observed values.

The following objective functions were used during the optimization process for this study:

1: the Nash and Sutcliffe (1970) coefficient of efficiency defined as:

$$E_{NS} = 1 - \frac{\sum_{i=1}^n (O_i - S_i)^2}{\sum_{i=1}^n (O_i - O_{ave})^2} \quad (2)$$

where O_i is the hourly i -th observed discharge, S_i is the simulated discharge, O_{ave} is the mean value of the observed discharges and n is the number of hourly values in the calibration data set. The coefficient of efficiency was selected because it is dimensionless and is easily interpreted. If the model predicts observed streamflow with perfection then $E_{NS}=1$. If $E_{NS}<0$ then the model's predictive power is worse than simply using the average of the observed values.

2: the relative bias (RB) defined as:

$$RB = \frac{\sum_{i=1}^n (S_i - O_i)}{\sum_{i=1}^n O_i} \quad (3)$$

RB is a measure of total volume difference between observed and simulated streamflows. Positive RB indicates overestimation of runoff, negative RB indicates underestimation of runoff.

A simple split sample test was used by dividing the available data into two sets, one used for parameter estimation (calibration period) and the other for model validation (validation period).

Detailed specific results are reported for six basins reported below. The six basins are:

- Aurino a S. Giorgio;
- Gadera a Mantana;
- Ridanna at Vipiteno;
- Rienza at Vandoies;
- Talvera at Bolzano;
- Rio Casies at Colle.

Overall results concerning the NS score and the relative bias (termed also as relative error) are reported in Table 2.



Tab. 2.: Information on discharge record and calibration/validation period.

Aurino a S. Giorgio			
	From date	To date	N-S / Rel.Error (%)
Available record*	01-Jan-2000	30-Sep-2011	-
Calibration period	01-Jul-2004	01-Jul-2007	0.83/-4.57
Validation period	01-Jul-2007	30-Oct-2010	0.89/2.19
Gadera at Mantana			
	From date	To date	N-S / Rel.Error (%)
Available record*	01-Jan-2000	30-Sep-2011	-
Calibration period	01-Jul-2004	01-Jul-2007	0.53/-5.29
Validation period	01-Jul-2007	30-Oct-2010	0.37/-2.05
Ridanna at Vipiteno			
	From date	To date	N-S / Rel.Error (%)
Available record*	01-Jan-2000	30-Sep-2011	-
Calibration period	01-Jul-2004	01-Jul-2007	0.71/-7.49
Validation period	01-Jul-2007	30-Oct-2010	0.79/-5.39
Rienza at Vandoies			
	From date	To date	N-S / Rel.Error (%)
Available record*	01-Jan-2000	30-Sep-2011	-
Calibration period	01-Jul-2004	01-Jul-2007	0.76/0.60
Validation period	01-Jul-2007	30-Oct-2010	0.81/5.74
Talvera at Bolzano			
	From date	To date	N-S / Rel.Error (%)
Available record*	01-Jan-2000	30-Sep-2011	-
Calibration period	01-Jul-2004	01-Jul-2007	0.52/-2.2
Validation period	01-Jul-2007	30-Oct-2010	0.53/-1.09
Casies at Colle			
	From date	To date	N-S / Rel.Error (%)
Available record*	01-Jan-2000	30-Sep-2011	-
Calibration period	01-Jul-2004	01-Jul-2007	0.53/11.6
Validation period	01-Jul-2007	30-Oct-2010	0.62/2.21

The soil moisture information used for debris flow analysis is supplied by the relative content of the PDM conceptual store. Obtained results are illustrated below.

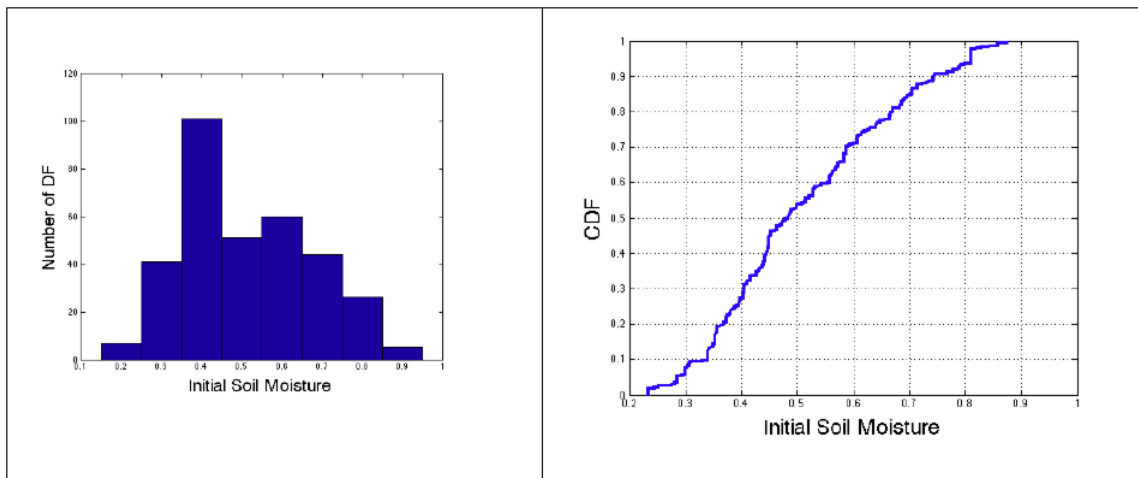


Fig. 7 Relationship between number of debris flows and initial soil moisture for the 405 debris flow events analysed in the ED30 archive.

Fig. 7 shows the relationship between number of debris flows and initial soil moisture for the 405 debris flow events analysed in the ED30 archive. The CDF curve shows that the median value for the initial soil moisture content is equal to 0.48.

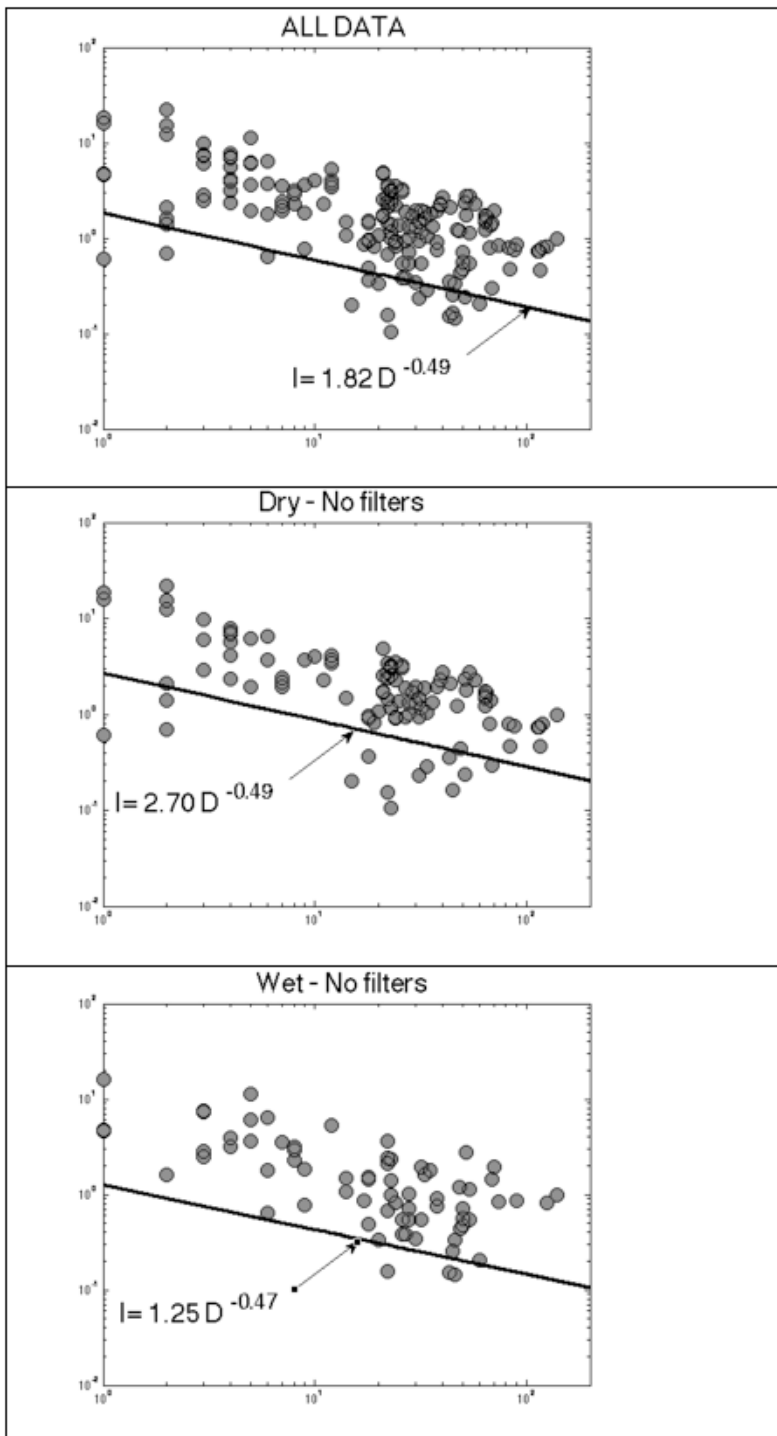


Fig. 8 ID relationship derived at 1% probability, based on: a) all data; b) dry events ($SM < 0.48$); c) wet events ($SM > 0.48$).

Fig. 8 shows the ID relationships obtained when the events are selected based on initial SM. As expected, lower precipitation thresholds are obtained for the wet case, which means that less precipitation is required to trigger debris flows than in the dry case. This supports the as-



assumption that debris flow triggering in the study area is influenced antecedent soil moisture, and provides a methodology to incorporate this information into the forecasting procedure. To this end, ATSOFT developed a system Graphical User Interface which permits to assess the severity of the initial soil moisture content, using a grading into three states which are discriminated at the catchment scale based on two soil moisture thresholds. The lower soil moisture threshold (termed Threshold_min) identifies soil moisture states that are very low and require very large precipitation depths to trigger debris flows and landslides. The higher soil moisture threshold (termed Threshold_max) identifies soil moisture states that are susceptible to trigger debris flows and landslides. This provides a graphic ranking system, as shows in Fig. 9 for an event occurred on Oct 1, 2010. According to this ranking system:

- Green colour identifies catchments characterised by soil moisture less than Threshold_min;
- Yellow colour identifies catchments characterised by soil moisture larger than Threshold_min and less than Threshold_max;
- Red colour identifies catchments characterised by soil moisture larger than Threshold_max.

Aggregation and ranking rules have been developed also to rank the so-called “forecasting regions”, i.e. aggregation of catchments which are characterized by similar hydrometeorological behaviours according to the synoptic and mesoscale forcings.

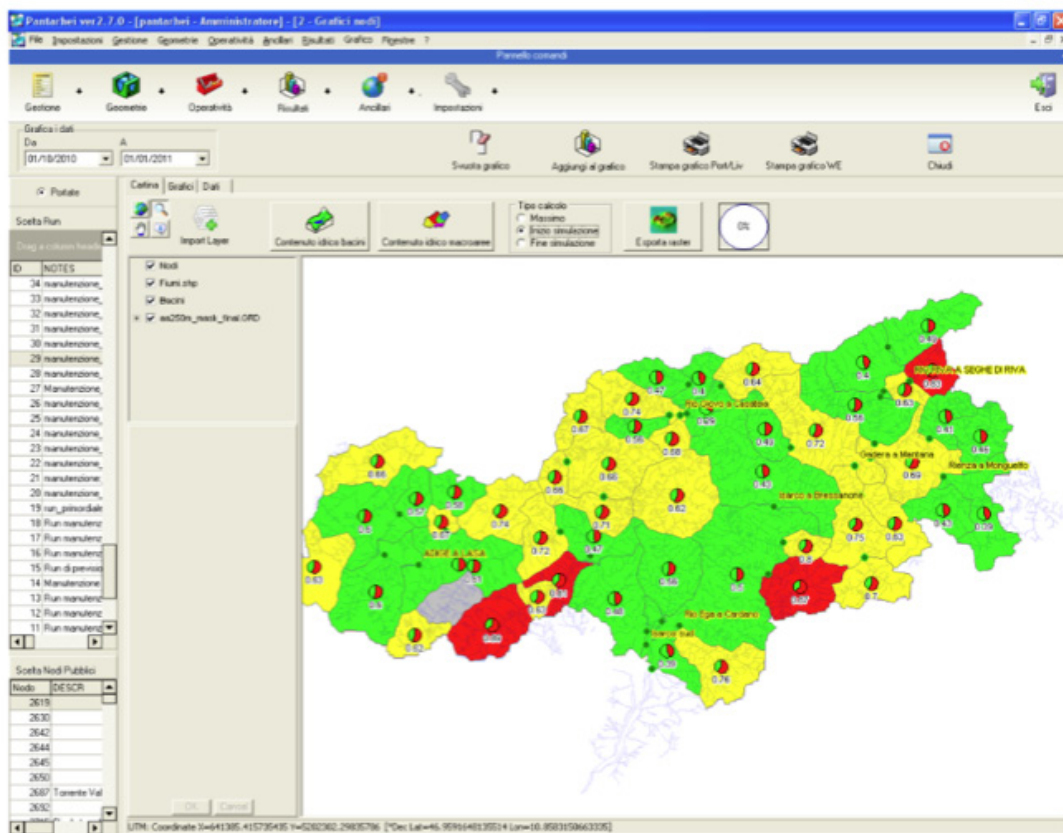


Fig. 9 Colour ranking system exemplified for the starting phase of the event occurred on October 1, 2010.



3. Extension of ICHYMOD to the simulation of glaciated catchment

The ICHYMOD snow routine has been extended to include the simulation of hydrological processes on the glacier surfaces. The following Sections describes the Snow/Glacier routine and provides a first assessment of the obtained results for the catchment of Noce Bianco at Pian Venezia.

3.1 Snow / Glacier routine for ICHYMOD

The following processes are included in the SNOW modelling procedure:

- Determination of the form of the precipitation;
- Correction for the aerodynamic effect around the precipitation gauges and poor representation of meteorological stations (precipitation undercatching);
- Computation of snowmelt;
- Estimation of retention and refreezing of liquid water in the snowpack;
- Snowmelt under rain conditions;
- Albedo: When it snows the albedo is set equal to the AlbSnow parameter, then it is reduced in time based on accumulated temperature.

1. The form of precipitation

The air temperature is used as a determining factor, meaning that a threshold temperature interval is used to distinguish between rainfall, snowfall and a mix of rain and snow.

2. Snowfall correction and rainfall correction

This correction is performed by multiplying the precipitation depth by a Snowfall Correction Factor (SCF). Precipitation is also corrected for poor representativeness of the raingauges by using a Rainfall Correction Factor (RCF).

3. Temperature index method for snowmelt computation

The snow routine represents snow accumulation and melt by using a distribution function approach based on a combined radiation index degree-day concept (Cazorzi and Dalla Fontana, 1986). The snowmelt rate M (mm h⁻¹) during day hours is given by:

$$M(t) = C_{CMF} \cdot E_{index} [T(t) - T_{cr}] \quad (4)$$

where:

C_{CMF} = Combined melt factor (mm/(°C MJ m⁻² giorno⁻¹));

E_{index} = Energy index;



$T(t)$ =temperature at time t ($^{\circ}\text{C}$).

The snowmelt rate M (mm h^{-1}) during night hours is given by:

$$M(t) = C_{CMF} \cdot E_{index,min} [T(t) - T_{cr}] \quad (5)$$

where:

$E_{index,min}$ = constant parameter.

With rainfall over snowpack, the melt is computed as follows:

Ne deriva la seguente formula ad indice termico:

$$M(t) = \left(R_{MF} + \frac{P(t)}{80.} \right) \cdot T(t) \quad (3)$$

where:

$P(t)$ is the rainrate at time t ;

R_{MF} =Rain Melt Factor.

4. Updating the snowpack water equivalent

The model computes the snowmelt contribution to runoff by updating the snow cover water equivalent, by using a water retention capacity in the snowpack .

When snowmelt starts, water is percolating through the snowpack. Some of this water will be retained by capillary forces and thus detain water yield into the river.

In ICHYMOD, a water holding capacity must be exceeded before the pack can yield any water (0.1 Water Equivalent). The melt content exceeding this threshold is propagated through the snowpack at a rate of 3 h/1000mmWE.

ICHYMOD includes also a refreezing routine, if snowmelt is interrupted by the intrusion of cold air. If so, the liquid water content is reduced and added to the snowpack (refreezing factor=0.03 $\text{mm}^{\circ}\text{C h}$).

a) Model Parameters

- **CriticalTemp** [$^{\circ}\text{C}$] Threshold to decide the phase of precipitation (fixed at 1.5 $^{\circ}\text{C}$).
- **BaseTemp** [$^{\circ}\text{C}$] Base Temperature T_{cr} is Eq. (1) and (2) (fixed at 0 $^{\circ}\text{C}$)
- **LiquidWater** [-] amount of liquid water stored in the snowpack, given as a fraction of the WE (fixed at 0.1)
- **DelayTime** [h/1000mmWE] dealy time to propagate melt water through the snowpack.
- **ReFreezing** [mm/ $^{\circ}\text{C h}$] Refreezing (fixed at factor 0.03).



The catchment-specific model parameters are:

- **SCF** [-] (Snow Correction Factor) this parameter is used to correct the undercatching of precipitation (it ranges between 1.5 and 2.5);
- **RCF** [-] (Rain Correction Factor) this parameter adjusts for orographic effects on liquid precipitation. It usually ranges between 1 and 1.3;
- **RMF** [mm/°C ora] (Rain Melt Factor) parameter which provides the melt amount when it rains over snow. The value is given equal to 0.3;
- **CMF** [mm m² giorno/(°C MJ ora)] (Combined Melt Factor) parameter used to simulate the melt amount given the air temperature.

State variables

The state variables are as follows:

- **WE** [mm] (Water Equivalent) given for each band;
- **LiqW** [mm] (Liquid Water) liquid water included into the snow cover for each band;
- **Melt** [mm] melt amount for each band;
- **Ice** [mm] melt refreezed for each band.

Modification for Glacier modelling

1. The Glacier modelling will start when WE is less than threshold;
2. The glacier extension is considered as fixed for a certain watershed;
3. If $P(t) > 0$, and precipitation is liquid, this is treated as rainfall on bare ground;
4. M is computed based on Eq. (1);
5. Albedo is included and is a constant parameter;
6. Two different values are considered for CMF for snow and for Glacier;
7. There is no propagation through the snowpack, no refreezing, no melt due to rain on snow. This means that the Glacier module will be equal to the snow module, but with a much less complex structure.
8. Glacier melt amount is treated as surface runoff, and propagated to the outlet using 2 linear reservoirs in series with parameter k_{Glac} .

New input data

1. Map of the glacier surface;
2. Albedo for glacier;
3. CMF values for glacier.



3.2 Model implementation

The model has been applied to model the partially glacierised basin of Noce Bianco at Pian Venezia, a 8.4 km² basin located on the Noce basin in Trentino (Fig. 10, 11 and Tab. 3). The main motivation for this choice is that the glacier melt application has been already applied in the catchment (Carturan et al., 2012) which permits to estimate the correct amount of precipitation over the basin for the years 2007-2009 (Tab. 4).

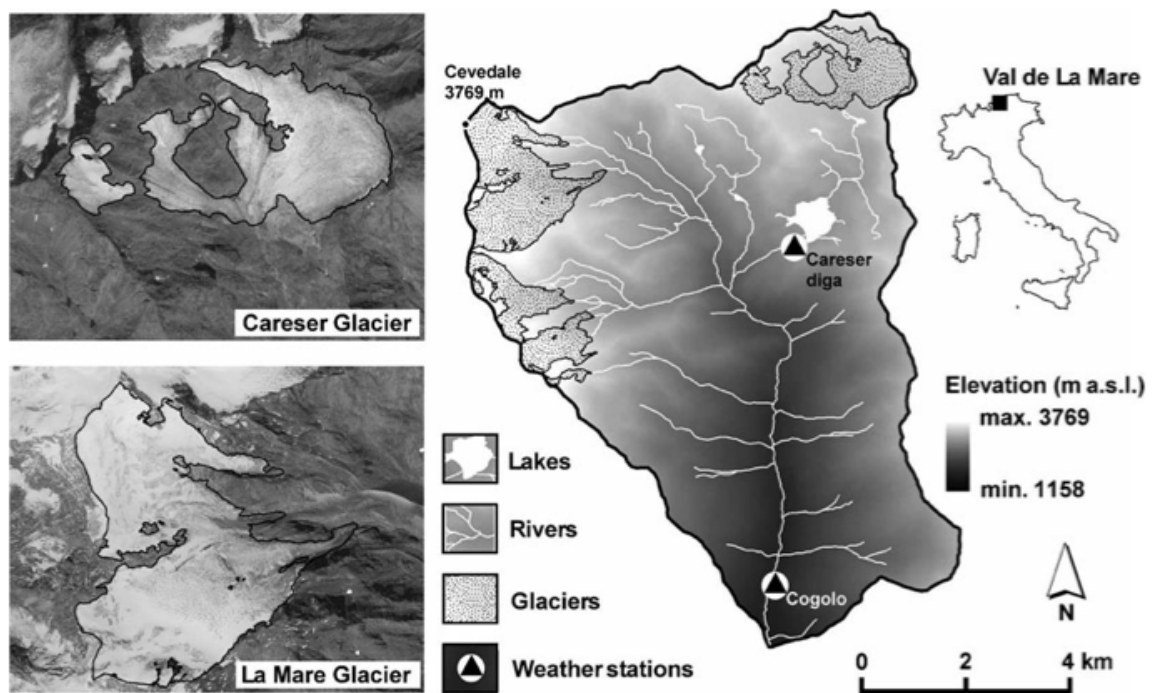


Fig. 10: Geographical setting of Val de la Mare and of Careser and La Mare glaciers.

The basin has been subdivided into 7 sub-basins (Tab. 3) and has been applied for the years 2008 and 2009.

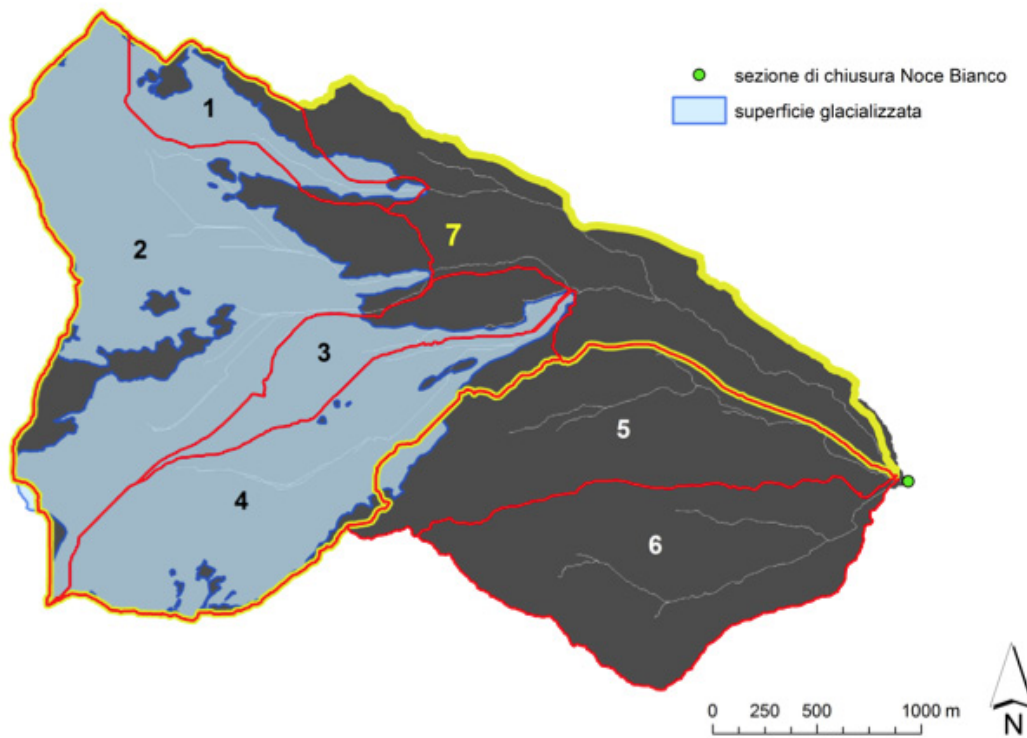


Fig. 11: Catchment of Noce Bianco at Pian Venezia, with the subdivision in sub-catchments used for the ICHYMOD implementation and verification.

Tab. 3: Noce Bianco at Pian Venezia: subdivision into sub-basins

Basin	Sureface(km2)	Glacer surface (km2)	Glacer surface (%)
1	0.41	0.28	69
2	2.40	1.93	80
3	0.50	0.32	65
4	1.28	1.15	90
5	1.20	0.05	4
6	1.31	-	-
7	5.85	3.72	64
Noce Bianco a Pian Venezia	8.38	3.77	45



Tab. 4: Data available for the model application.

Year	Temperature		Precipitation		Discharge
	Caser Diga	Cogolo	Caser Diga	Cogolo	Magra
2002	25%	25%	25%	25%	
2003	100%	100%	100%	100%	
2004	100%	100%	100%	100%	
2005	100%	100%	100%	100%	
2006	100%	100%	100%	100%	
2007	100%	100%	100%	100%	38%
2008	100%	100%	100%	100%	100%
2009	74%	74%	74%	74%	80%

A first assessment of the model application is reported in Fig. 12, showing that the model is able to simulate accurately the hydrological dynamics at both the seasonal and daily temporal scale.

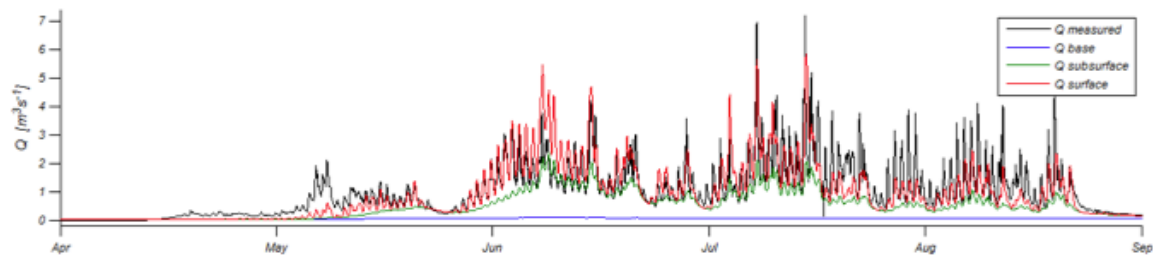


Fig. 12: Observed and simulated discharges for Noce at Pian Venezia for the Year 2008.

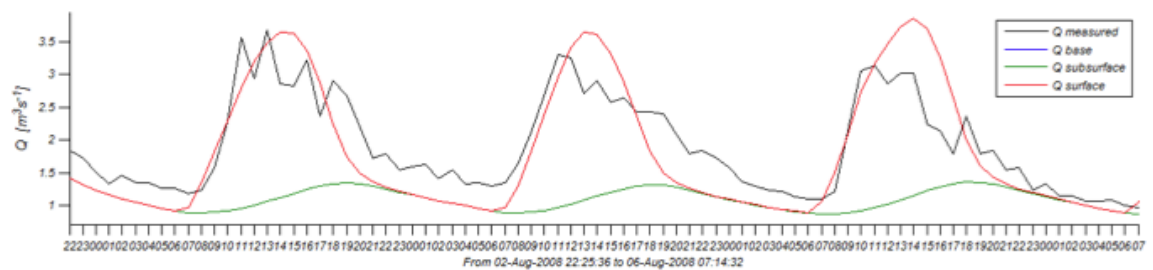


Fig. 13: Observed and simulated discharges for Noce at Pian Venezia for three days in August 2008.

An example of hourly simulation for three consecutive days is reported in Fig. 13, with peaks which are generated by daily glacier melt. The simulation shows that the model is able to reproduce accurately both the discharge peak and the time of the peak.



4. Extension of ICHYMOD to the simulation of artificial reservoir systems

In this section, we describe the modifications developed on the ICHYMOD model to account for the operations on the complex system of 8 hydropower reservoirs.

The reservoirs are listed in Table 5, where sub-basins that should be include into a new topology are marked in bold.

Tab. 5: Reservoirs included into ICHYMOD and in the ARFFS system

River	Station
Resia	Glorenza
Gioveretto	Lasa
Zoccolo	S Pancrazio
Alborelo	Lana
Neves	Selva Molini
Verbago	Naturno
Fortezza	Rio Pusteria/Bressanone
Monguelfo	Brunico

Given the complexity of the changes required at this point, a separate report is dedicated to the description of the changes required for both ICHYMOD and ARFFS.



References

- Anagnostou, M.N., Kalogiros, J., Anagnostou, E.N., Tarolli, M., Papadopoulos, A. and Borga, M., 2010. Performance evaluation of high-resolution rainfall estimation by X-band dual polarization radar for flash flood applications in mountainous basins. *Journal of Hydrology* 394 (1–2), 4–16, doi:10.1016/j.jHydrology2010.06.026.
- Andrieu, H. and Creutin, J.D., 1995. Identification of Vertical Profiles of Radar Reflectivity for Hydrological Applications Using an Inverse Method. Part I: Formulation. *Journal of Applied Meteorology* 34, 225–239.
- Baum, R.L., Godt, J.W. and Savage, W.Z., 2010. Estimating the timing and location of shallow rainfall-induced landslides using a model for transient, unsaturated infiltration. *Journal of Geophysical Research* 115(F3):F03013.
- Bellon, A., Lee, G., and I. Zawadzki, 2005: Error statistics of VPR corrections in stratiform precipitation. *Journal of Applied Meteorology* 44,998–1015.
- Berne, A. and Krajewski, W.F., 2013. Radar for hydrology: unfulfilled promise or unrecognized potential? *Advances in Water Resources* 51, 357–366.
- Borga M. and A. Vizzaccaro, 1997: On the interpolation of hydrologic variables: formal equivalence of multiquadratic surface fitting and kriging. *Journal of Hydrology*, 195, 160-171, 1997.
- Borga, M., E.N. Anagnostou, G. Blöschl, J-D. Creutin, 2011: Flash flood forecasting, warning and risk management: the HYDRATE project. *Environmental Science & Policy*, 14, 834-844.
- Borga, M., 2002: Accuracy of radar rainfall estimates for streamflow simulation. *Journal of Hydrology*, 267, 26-39.
- Borga, M., Dalla Fontana, G., Gregoret, C. and Marchi, L., 2002. Assessment of shallow landsliding by using a physically based model of hillslope stability. *Hydrological Processes* 16 (14), 2833-2851.
- Borga, M., S. Degli Esposti and D. Norbiato, 2006: Influence of errors in radar rainfall estimates on hydrological modelling prediction uncertainty. *Water Resources Research*, 42, W08409, doi:10.1029/2005WR004559.
- Borga, M., Stoffel, M., L. Marchi, F. Marra and M. Jakob, 2014. Hydrogeomorphic response to extreme rainfall in headwater systems: flash floods and debris flows. *Journal of Hydrology*, in print.
- Bouilloud, L., Delrieu, G., Boudevillain, B., Borga, M. and Zanon, F., 2009. Radar rainfall estimation for the post-event analysis of a Slovenian flash-flood case: application of the mountain reference technique at C-band frequency. *Hydrology and Earth System Sciences* 13, 1349–1360.
- Brunetti, M.T., Peruccacci, S., Rossi, M., Luciani, S., Valigi, D. and Guzzetti, F., 2010. Rainfall thresholds for the possible occurrence of landslides in Italy. *Natural Hazards and Earth System Science* 10(3), 447–458.
- Caine, N., 1980. The rainfall intensity-duration control of shallow landslides and debris flows. *Geografiska Annaler* 62A, 23-27.
- Cannon, S.H. and Gartner, J.E., 2005. Wildfire-related debris flow from a hazards perspective. In: Jakob M, Hungr O, (eds), *Debris flow hazards and related phenomena*. Berlin Heidelberg: Springer, 363–385.
- Carturan, L., Cazorzi, F., Dalla Fontana, G., 2012: Distributed mass-balance modelling on two neighbouring glaciers in Ortles-Cevedale Italy, from 2004 to 2009. *Journal of Glaciology*, 58 (209), 467-486.
- Cazorzi, F., Dalla Fontana, G., 1996: Snowmelt modelling by combining air temperature and a distributed radiation index. *Journal of Hydrology*, 181 (1-4), 169-187.
- Chen, C.Y., Lin, L.Y., Yu, F.C., Lee, C.S., Tseng, C.C., Wang, A.H. and Cheung, K.W., 2007. Improving debris flow monitoring in Taiwan by using high-resolution rainfall products from QPESUMS. *Natural Hazards* 40(2), 447–461.
- Chen, J.C., Huang, W.S., Jan, C.D. and Tsai, Y.F., 2011. Rainfall conditions for the initiation of debris flows during Typhoon Morakot in the Chen-Yu-Lan watershed in Central Taiwan. In: 5th International Conference on Debris-Flow Hazards Mitigation: Mechanics, Prediction and Assessment, edited by Genevois, R., Hamilton, D.L., and Prestininzi, A., Casa Editrice, Università La Sapienza, Roma, 31-36.
- Chiang, S.-H. and Chang, K.-T., 2009. Application of radar data to modeling rainfall-induced landslides. *Geomorphology*, 103 (3), 299-309.
- Da Ros D. and M. Borga, 1997: Use of digital elevation model data for the derivation of the geomorphologic instantaneous unit hydrograph. *Hydrological Processes*, 11, 13-33, 1997.
- D'Agostino, V. and Marchi, L., 2001. Debris flow magnitude in the Eastern Italian Alps: Data Collection and Analysis. *Physics and Chemistry of the Earth* 26(9), 657-663.



- David-Novak, H.B., Morin, E. and Enzel, Y., 2004. Modern extreme storms and the rainfall thresholds for initiating debris flows on the hyperarid western escarpment of the Dead Sea, Israel. *Bulletin of the Geological Society of America*, 116(5-6), 718–728.
- Delrieu, G., Creutin, J.D., and Saint-Andre, I., 1991. Mean K-R relationships: practical results for typical weather radar wavelengths. *Journal of Atmospheric and Oceanic Technology* 8, 467-476.
- Delrieu, G., Serrar, S., Guardo, E. and Creutin, J.D., 1999. Rain measurement in hilly terrain with X-band radar systems: Accuracy of path-integrated attenuation estimates derived from mountain returns. *Journal of Atmospheric and Oceanic Technology* 16, 405–416.
- Frei, C., Schär, C., 1998. A precipitation climatology of the Alps from high-resolution rain-gauge observations. *International Journal of Climatology* 18 (8), 873-900.
- Germann, U., 1999: Radome attenuation - a serious limiting factor for quantitative radar measurements? *Meteorologische Zeitschrift* 8, 85–90.
- Germann, U., Galli, G., Boscacci, M., Bolliger, M., 2006: Radar precipitation measurement in a mountainous region. *Quarterly Journal of the Royal Meteorological Society* 132 (618 A), 1669-1692.
- Godt, J.W., Baum, R.L. and Chleborad, A.F., 2006. Rainfall characteristics for shallow landsliding in Seattle, Washington, USA. *Earth Surface Processes and Landforms* 31(1), 97–110.
- Gourley, J.J., Hong, Y., Flamig, Z.L., Wang, J., Vergara, H. and Anagnostou, E.N., 2011. Hydrologic evaluation of rainfall estimates from radar, satellite, gauge, and combinations on Ft. Cobb basin, Oklahoma. *Journal of Hydrometeorology*, 12 (5), pp. 973-988.
- Guzzetti, F., Cardinali, M., Reichenbach, P., Cipolla, F., Sebastiani, P., Galli, M. and Salvati, P., 2004. Landslides triggered by the 23 November 2000 rainfall event in the Imperia Province, Western Liguria, Italy. *Engineering Geology* 73(3-4), 229–245.
- Guzzetti, F., Peruccacci, S., Rossi, M. and Stark, C.P., 2007. Rainfall thresholds for the initiation of landslides in central and southern Europe. *Meteorology and Atmospheric Physics*, 98, 239-267.
- Guzzetti, F., Peruccacci, S., Rossi, M., and Stark, C.P., 2008. The rainfall intensity–duration control of shallow landslides and debris flows: an update. *Landslides* 5, 3–17, DOI 10.1007/s10346-625 007-0112-1.
- Guzzetti, F., Reichenbach, P., Cardinali, M., Galli, M. and Ardizzone, F., 2005. Probabilistic landslide hazard assessment at the basin scale. *Geomorphology* 72 (1-4), 272-299.
- Iverson, R.M., Reid, M.E. and LaHusen, R.G., 1997. Debris-flow mobilization from landslides. *Annual Reviews of Earth and Planetary Sciences* 25, 85–138.
- Jakob, M. and Weatherly, H., 2003. A hydroclimatic threshold for landslide initiation on the North Shore Mountains of Vancouver, British Columbia. *Geomorphology* 54(3-4), 137–156.
- Jakob, M., Owen, T. and Simpson, T., 2012. A regional real-time debris-flow warning system for the District of North Vancouver, Canada., *Landslides* 9 (2), 165-178.
- Krajewski, W.F., Ntelekos, A.A. and Goska, R., 2006. A GIS-based methodology for the assessment of weather radar beam blockage in mountainous regions: two examples from the US NEXRAD network. *Computer and Geosciences* 32, 283-302.
- Marra, F., 2013. Procedura integrata di analisi e correzione delle osservazioni radar per la stima di precipitazioni intense in ambiente alpino. PhD Thesis, University of Padova, Italy, 154 pp. (in Italian).
- Marra, F., E. I. Nikolopoulos, J. D. Creutin, M. Borga, 2014: : Radar rainfall estimation for the identification of debris-flow occurrence thresholds. *Journal of Hydrology*, conditionally accepted.
- Mei, Y., Anagnostou, E.N., Nikolopoulos, E.I., Borga, M., 2014. Error Analysis of Satellite Rainfall Products in Mountainous Basins. *J. Hydrometeor* 140508110258003. doi:10.1175/JHM-D-13-0194.1
- Nikolopoulos, E.I., Crema S., Marchi L, Marra F., Guzzetti F. and Borga M., 2014. Impact of uncertainty in rainfall estimation on the identification of rainfall thresholds for debris-flow occurrence. *Geomorphology*, 221, 286-297, ISSN 0169-555X, <http://dx.doi.org/10.1016/j.geomorph.2014.06.015>.
- Norbiato, D., Borga, M., Merz, R., Blöschl, G. and Carton, A., 2009. Controls on event runoff coefficients in the eastern Italian Alps. *Journal of Hydrology* 375 (3-4), 312-325.
- Norbiato, D., M. Borga and R. Dinale, 2009b: Flash flood warning in ungauged basins by use of the Flash Flood Guidance and model-based runoff thresholds. *Meteorological Applications*, 16(1), 65-75, .DOI: 10.1002/met.126; <http://dx.doi.org/10.1002/met.126>.
- Norbiato, D., M. Borga, R. Merz, G. Blöschl and A. Carton, 2009a: Controls on event runoff coefficients in the eastern Italian Alps. *Journal of Hydrology*, 375, 312-325, doi:10.1016/j.jhydrol.2009.06.044.



- Norbiato, D., M. Borga, S. Degli esposti, E. Gaume, S. Anquetin, 2007: Flash flood warning based on rainfall depth-duration thresholds and soil moisture conditions: An assessment under European conditions. *J. Hydrology*, 274-290, 10.1016/j.jhydrol.2008.08.023.
- Pavlova, I., Jomelli, V., Grancher, D., Brunstein, D. and Vrac, M., 2011. Debris flow occurrence and meteorological factors in the French Alps: a regional investigation. In: Genevois R., Hamilton D.L., and Prestininzi A. (eds), 5th International Conference on Debris flow Hazards Mitigation: Mechanics, Prediction and Assessment, Casa Editrice Università La Sapienza, Roma, 127-134, DOI: 10.4408/IJEGE.2011-03.B-015.
- Peleg, N., Ben-Asher, M. and Morin, E., 2013. Radar subpixel-scale rainfall variability and uncertainty: lessons learned from observations of a dense rain-gauge network. *Hydrology and Earth System Sciences*, 17, 2195-2208.
- Pellarin, T., Delrieu, G. and Saulner, G.M., 2002. Hydrologic visibility of weather radar systems operating in mountainous regions: case study for the Ardeche catchment (France). *Journal of Hydrometeorology* 3, 539-555.
- Peruccacci, S., Brunetti, M.T., Luciani, S., Vennari, C. and Guzzetti, F., 2012. Lithological and seasonal control on rainfall thresholds for the possible initiation of landslides in central Italy. *Geomorphology* 139-140, 79-90.
- Reichenbach, P., Cardinali, M., De Vita, P. and Guzzetti, F., 1998. Regional hydrological thresholds for landslides and floods in the Tiber River Basin (central Italy), *Environmental Geology* 35, 146-159.
- Ruiz-Villanueva, V., Borga, M., Zoccatelli, D., Marchi, L., Gaume, E. and Ehret, U., 2012. Extreme flood response to short-duration convective rainfall in South-West Germany, *Hydrology and Earth System Sciences* 16, 1543-1559.
- Saito, H., Nakayama, D. and Matsuyama, H., 2010. Relationship between the initiation of a shallow landslide and rainfall intensity-duration thresholds in Japan. *Geomorphology* 118(1-2), 167-175.
- Salvati, P., Bianchi, C., Rossi, M. and Guzzetti, F., 2010. Societal landslide and flood risk in Italy. *Natural Hazards and Earth System Science*, 10 (3), 465-483.
- Schneuwly-Bollschweiler, M. and Stoffel, M., 2012. Hydrometeorological triggers 665 of periglacial debris flows – a reconstruction dating back to 1864. *Journal of Geophysical Research – Earth Surface* 117, F02033.
- Stoffel, M., Bollschweiler, M. and Beniston, M., 2011. Rainfall characteristics for periglacial debris flows in the Swiss Alps: past incidences – potential future evolutions. *Climatic Change* 105, 263-280.
- Tabios GQ III, Salas JD, 1985: A comparative analysis of techniques for spatial interpolation of precipitation. *Water. Resour. Bull.*, 21(3), 365-380.
- Tarolli, P., Borga, M., Chang, K-T. and Chiang, S., 2011: Modelling shallow landsliding susceptibility by incorporating heavy rainfall statistical properties. *Geomorphology* 133, 3-4, 199-211.
- Villarini, G. and Krajewski, W.F., 2010. Review of the different sources of uncertainty in single polarization radar-based estimates of rainfall. *Surveys in Geophysics* 31 (1), 107-129.
- Villarini, G., Mandapaka, P.V., Krajewski, W.F. and Moore, R.J., 2008. Rainfall and sampling errors: a rain gauge perspective. *Journal of Geophysical Research* 113 D11102, doi:10.1029/2007JD009214.
- Wieczorek G.F. and Glade T., 2005. Climatic factors influencing occurrence of debris flows. In: Jakob M, Hungr O (eds) *Debris flow hazards and related phenomena*. Berlin, Springer, 325-362.
- Wieczorek, G.F., 1996. Landslide triggering mechanisms. In: *Landslides: Investigation and Mitigation* (TurnerAK, Schuster RL, eds). Washington DC: Transportation Research Board, National Research Council, Special Report, 76-90.
- Wieczorek, G.F., Morgan, B.A. and Campbell, R.H., 2000. Debris-flow hazards in the Blue Ridge of central Virginia. *Environmental and Engineering Geoscience* 6(1), 3-23.

